CHIN. PHYS. LETT. Vol. 37, No. 6 (2020) 066803

Express Letter

Water-Mediated Spontaneously Dynamic Oxygen Migration on Graphene Oxide with Structural Adaptivity for Biomolecule Adsorption *

Yusong Tu(涂育松)[1,2**], Liang Zhao(赵亮)[1], Jiajia Sun(孙佳佳)[1], Yuanyan Wu(吴园燕)[1], Xiaojie Zhou(周晓洁)[3], Liang Chen(陈亮)[4], Xiaoling Lei(雷晓玲)[5,6], Haiping Fang(方海平)[5,6], Guosheng Shi(石国升)[7**]

[1]*College of Physics Science and Technology, Yangzhou University, Jiangsu 225009, China*
[2]*Key Laboratory of Polar Materials and Devices (Ministry of Education), Department of Optoelectronics, East China Normal University, Shanghai 200062, China*
[3]*National Facility for Protein Science in Shanghai, Shanghai Advanced Research Institute, Chinese Academy of Sciences, Shanghai 201210, China*
[4]*Department of Optical Engineering, Zhejiang A&F University, Lin'an 311300, China*
[5]*Department of Physics, East China University of Science and Technology, Shanghai 200237, China*
[6]*Division of Interfacial Water and Key Laboratory of Interfacial Physics and Technology, Shanghai Institute of Applied Physics, Chinese Academy of Sciences, Shanghai 201800, China*
[7]*Shanghai Applied Radiation Institute, Shanghai University, Shanghai 200444, China*

(Received 7 May 2020)

We theoretically and experimentally show that, with water being adsorbed, the graphene oxide (GO) is converted to a spontaneously dynamic covalent material under ambient conditions, where the dominated epoxy and hydroxyl groups are mediated by water molecules to spontaneously break/reform their C–O bonds to achieve dynamic oxygen migration. This dynamic material presents structural adaptivity for response to biomolecule adsorption. Both density functional theory calculations and ab initio molecular dynamics simulations demonstrate that this spontaneously dynamic characteristics is attributed to the adsorption of water molecules, which sharply reduces the barriers of these oxygen migration reactions on GO to the level less than or comparable to the hydrogen bonding energy in liquid water.

PACS: 68.37.−d, 68.90.+g, 61.48.Gh, 87.90.+y DOI: 10.1088/0256-307X/37/6/066803

Large-area dynamic covalent new materials that are elaborately adaptive and responsive to their surroundings have shown great potential in new technologies and can be used in a variety of desired applications,[1−4] such as molecular detection and recognition,[5] (bio)sensors,[6] controlled drug delivery and release,[7] and dynamic-responsive systems.[8] In the past decade, there have been great efforts to exploit various reversible covalent reactions to achieve structural adaptivity in dynamic materials,[9−12] including nucleophilic aromatic substitution,[10] imine condensation,[11,13] disulfide exchange,[12] acetals,[14] olefin,[15] and alkyne metathesis.[16] However, these covalent reactions have usually relied on catalysis[4,9,12,14−16] or temperature[10,11] or pH[12,13] conditions to enable the formation of dynamic reversible covalent bonds. So far, it remains a large challenge to achieve a spontaneously dynamic material with reversible covalent reactions under ambient conditions, leading to a continuous change in constitution and offering structural adaptivity in practical applications.

Graphene oxide (GO) is an atom-thick sheet of carbon that is covalently functionalized with rich oxygen-containing groups dominated by epoxy and hydroxyl on its basal plane,[17−20] and it has great potential applications in areas such as molecular detection and sensors,[21−23] electronics and photonics,[24] catalysis,[25] biological and medical technologies,[26−29] and water treatment systems.[30,31] The functional oxygen groups are of fundamental importance to the properties and relevant applications of GO, as they allow for extensive interactions of GO with various molecules including biomolecules.[22−28,32,33] For examples, for biomedical applications, these covalent groups afford a vital improvement of GO water solubility and biocompatibility and provide intrinsic advantages to GO as smart platforms for biosensing, biomedical imaging, drug delivery and cancer treatment.[26,32] Generally, these functional oxygen groups seldom change or move along the basal plane of GO under ambient conditions,[34−36] if these functional oxygen groups can spontaneously move on GO, this would significantly change the relevant electrical, mechanical, and thermal properties of GO as well as expand GO-based relevant appli-

*Supported by the National Natural Science Foundation of China (Grant Nos. 11675138, 11705160, 11605151, U1832150, U1932123 and 11974366), the National Science Fund for Outstanding Young Scholars (Grant No. 11722548), the Key Research Program of Chinese Academy of Sciences (Grant No. QYZDJ-SSW-SLH053), the Fundamental Research Funds for the Central Universities, the Special Program for Applied Research on Supercomputation of the NSFC-Guangdong Joint Fund (the second stage), Supercomputer Center of CAS, and the BL01B Beamline of NFPS at SSRF.

**Corresponding author. Email: ystu@yzu.edu.cn; gsshi@shu.edu.cn

© 2020 Chinese Physical Society and IOP Publishing Ltd

cations. Here, we combine theoretical calculations and experimental observations to show that, with water being adsorbed, the GO is converted to a spontaneously dynamic covalent material under ambient conditions and presents structural adaptivity for response to biomolecule adsorption, where the epoxy and hydroxyl groups are mediated by water molecules to spontaneously break/reform their C–O bonds to achieve dynamic oxygen migration. To the best of our knowledge, this is the first report of a large-area spontaneously dynamic covalent molecular interface under ambient conditions.

We have performed density functional theory (DFT) calculations at the B3LYP/6-31G(d) level of theory (see PS1 in the Supplemental Material (SM)). In previous DFT calculations, the C–O bond breaking/reforming reactions in epoxy and hydroxyl groups on GO without water were found to have relatively high barriers.[34,35] To study the oxygen migration on GO, we further analyzed the C–O bond reaction of epoxy and the proton transfer between epoxy and hydroxyl for the exchange (see PS2 in the SM). As shown in Fig. 1(a), the C–O bond reactions have a much lower barrier of 3.9 kcal/mol for epoxy movement assisted by hydroxyl, but there remains a high barrier of 15.9 kcal/mol for proton transfer between the neighboring epoxy and hydroxyl for the exchange. Both barriers along the pathways indicate the local mobility of epoxy around its neighboring hydroxyl but little mobility of hydroxyl, which is consistent with the previous TEM observations.[36] Therein, an intermediate with one hanging oxygen atom single-bonded onto GO is observed, but this was easy to transform back into epoxy with thermal disturbance.

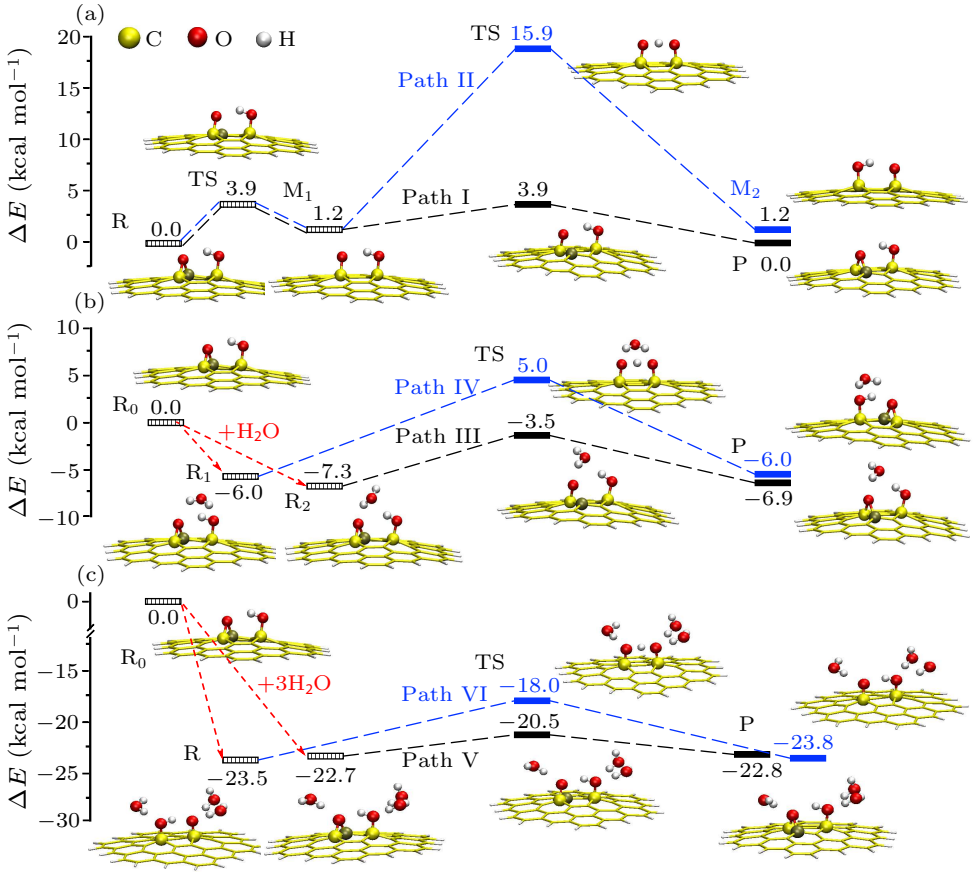

Fig. 1. (a) Oxygen migration pathways on GO without adsorbed water. The epoxy assisted with the hydroxyl moves by C–O bond breaking/reforming (path I, black) and the hydroxyl moves by proton transfer to the epoxy and exchange with each other (path Ⅱ, blue). Notation: relevant reactants (R), intermediate (M), transition states (TS), and products (P). (b) Pathways Ⅲ and Ⅳ, with one water adsorbed. (c) Pathways V and Ⅵ, with three waters adsorbed. The reactions passing through the intermediate in (b) and (c) are omitted for simplification.

We analyzed again the above pathways after adding water to GO and found that the water adsorption induces oxygen migration reactions along the pathways. As shown in Fig. 1, with only one water molecule adsorbed, the epoxy and hydroxyl movements along paths Ⅲ and Ⅳ have energy barriers of −3.5 kcal/mol and 5.0 kcal/mol, respectively, and with three water molecules adsorbed, all their barriers are far below zero along paths V and Ⅵ. Compared to the barrier without water adsorbed (path Ⅱ), the adsorption of one, two, and three water molecules reduce the barrier for proton transfer by

4.9 kcal/mol (path Ⅳ), 7.7 kcal/mol (Fig. S1 in the SM) and 10.1 kcal/mol (path Ⅵ), respectively. Notably, the adsorption of three water sharply reduces the barriers of both hydroxyl and epoxy movements down to 5.8 kcal/mol and 2.2 kcal/mol, respectively (see Fig. 1(c) and Fig. S2 in the SM). We note that the hydrogen bond energy is ∼5 kcal/mol in liquid water;[37] thus these barriers are less than or comparable to the hydrogen bond energy, indicating that movements can occur spontaneously under ambient conditions. These results indicate that water activation induces the hydroxyl movement via the exchange with epoxy by proton transfer and further expands the original local mobility of epoxy on GO without adsorbed water. In addition, we have also check possible oxygen migration pathways in between GO layers, and found that water adsorption increases interlayer spacings and prevents direct oxygen migration in between GO layers (see PS4 in the SM).

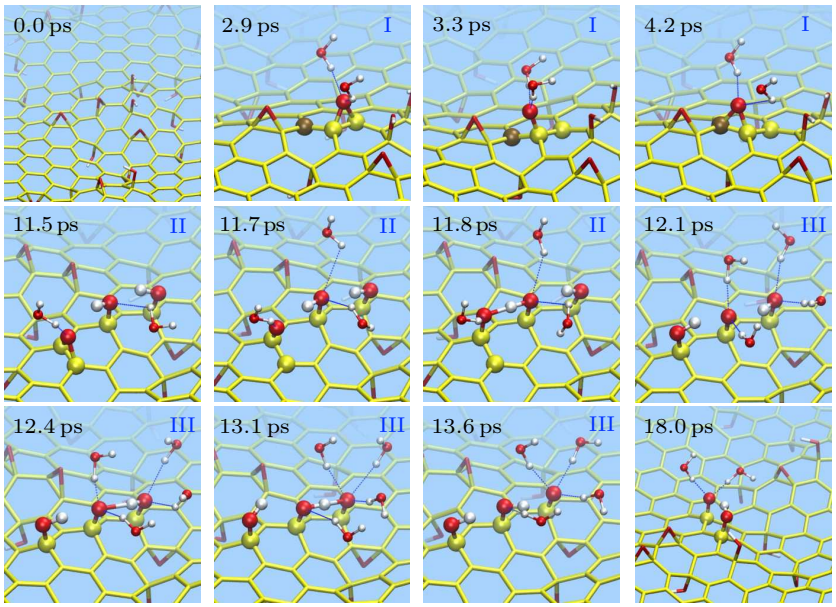

Fig. 2. Representative AIMD trajectory of oxygen migration in epoxy and hydroxyl groups on the basal plane of GO. Three reaction processes are denoted by reactions I, Ⅱ, and Ⅲ, and the numbers indicate the time of snapshots. Atom representations are the same as those in Fig. 1.

Unbiased *ab initio* molecular dynamics (AIMD) simulations further confirmed the spontaneously dynamic oxygen migration on GO, surrounded by liquid water with a density of ∼1.0 g/ml (corresponding to ambient conditions) (see the detailed AIMD Methods, PS5 in the SM). Figure 2 shows the representative AIMD trajectory with three reactions, denoted by I, Ⅱ, and Ⅲ (see movie S1 in the SM). In the snapshots from 2.9 ps to 4.2 ps (reaction I), we can see the epoxy moving process assisted directly by water molecules and not assisted by the neighboring hydroxyl (see paths I, Ⅲ, and V in Fig. 1). The snapshots from 11.5 ps to 18.0 ps present the hydroxyl movement via two successive proton-transfer reactions to exchange with epoxy (reactions Ⅱ and Ⅲ). We can clearly see the rearrangement of water molecules with dynamic orientations around the reaction intermediates. Further DFT calculations have also verified the pathway of reactions Ⅱ and Ⅲ by optimizing the analogous local reaction conformations of GO (see Fig. S5 in the SM). Interestingly, it can be seen that the intermediate remains with the assistance of water molecules and neighboring hydroxyl (see snapshots from 13.6 ps to 18.0 ps) (see Fig. 1(a)). All these reaction dynamics present in the AIMD simulations agree with the pathways based on DFT calculations, indicating a spontaneously dynamic oxygen migration on GO induced by water adsorption.

To check the dynamic oxygen migration on GO, *in situ* synchrotron radiation-based Fourier transform infrared (SR-FTIR) spectroscopy experiments have been carried out (see PS8 in the SM). We used GO membranes from GO suspensions with the drop-casting method[38–40] that has been widely used in characteristic studies and applications of GO.[30,41] The GO membranes were dried under an infrared lamp for ∼30 min and then sealed hermetically in dry nitrogen environments (fully dry GO membrane) as a control. The dried GO membranes were also kept under ambient conditions (dry GO membrane) and further were treated *in situ* by being immersed in a deionized water droplet of 20 μL for ∼10 min (wet GO membrane) (see PS9 and PS11 in the SM). These GO membranes were analyzed by *in situ* SR-FTIR experiments to detect the chemical oxygen distributions above them.

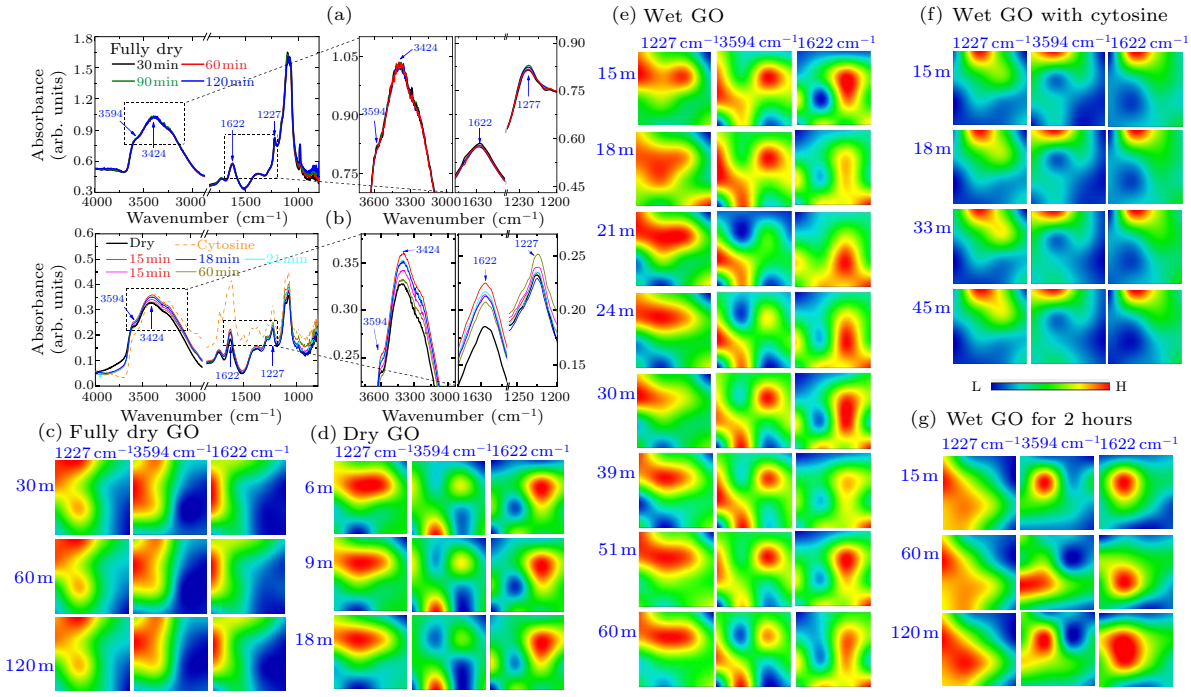

Fig. 3. *In situ* SR-FTIR spectra acquired from the fully dry GO membrane (a), and from the dry GO membrane, the wet GO membrane and the wet GO membrane with cytosine adsorbed (b). Two dotted-box regions of interest in the left subfigures are enlarged to show on the right. Characteristic IR peaks occur in the GO spectra at ∼1227 cm^{-1}, ∼1622 cm^{-1}, ∼3424 cm^{-1}, and ∼3594 cm^{-1}, and peaks occur in the spectra of GO with cytosine adsorbed at ∼3220 cm^{-1} and 1500 cm^{-1}. (c)–(g) Sequence of *in situ* images for 2D chemical distributions over the sampling area, on the fully dry GO membrane, on the dry GO membrane, on the wet GO membrane, on the wet GO membrane with cytosine adsorbed, and on the wet GO membrane for two-hour measurements at 1227 cm^{-1}, 1622 cm^{-1}, and 3594 cm^{-1}. The left numbers denote the time of the sequence in units of minute.

Figures 3(c), 3(d) and 3(e) show the sequent 2D chemical distributions of the epoxy (C–O–C, left) and hydroxyl (O–H, mid) groups, as well as the mixed contents of aromatic rings (C=C) and water (right), over a sampling area of 30 × 30 μm^2 (see PS10 in the SM also over a large sampling area of 90 × 90 μm^2) on the fully dry, dry and wet GO membranes, respectively. As shown in Fig. 3(e) for the wet GO membrane, the red region indicating high epoxy content is frequently stretched, and the red regions indicating high hydroxyl content and mixed content are also stretched, even extending to two or three separated regions in comparison with the corresponding regions on the dry membrane over time. This represents the significant changes in the epoxy and hydroxyl content after adding water to the dry membrane. In contrast, Fig. 3(d) shows that these regions on the dry GO membrane remain almost unchanged with time. Particularly as an important control, on the fully dry GO membrane sealed hermetically in dry nitrogen environments, the 2D distributions of hydroxyl and epoxy contents remain almost unchanged with time (see Fig. 3(c) and PS11 in the SM for details). Further, examining the hydroxyl content on the wet membrane as an example, the top-right red region is converted to green at 21 min, reappears at 30 min, but is shrunk at 60 min. This represents a periodically oscillational change in the hydroxyl contents (see the mid-sequence images of Fig. 3(e)). Figure 3(g) further demonstrates that real-time periodical oscillations in the distributions on the wet membrane have been retained for the whole time period of experimental observations (two hours) (also see PS10 in the SM). These real-time changes and oscillations in the distributions of the epoxy and hydroxyl contents demonstrate that the addition of water induces spontaneously dynamic movements of epoxy and hydroxyl on wet GO membranes.

To present the influence of water on the epoxy and hydroxyl spectra, we analyze the characteristic peaks of the corresponding groups. Figure 3(a) and 3(b) together with the relevant enlargements show four characteristic IR peaks, at ∼1227 cm^{-1} (C–O–C stretching of epoxy), ∼1622 cm^{-1} (C=C stretching of aromatic ring and deformation vibration of adsorbed water), ∼3424 cm^{-1} (stretching vibration of adsorbed water), and ∼3594 cm^{-1} (O–H stretching of hydroxyl).[42,43] Compared with the spectrum on the dry GO membrane, the peak at ∼3424 cm^{-1} is enhanced after adding water to the GO membrane but decreases over time and approaches the corresponding intensity of the dry membrane, indicating a loss of the water from GO due to evaporation. The peak at ∼1622 cm^{-1} is also enhanced after adding water,

but it maintains a relatively higher intensity, indicating a certain residual of water between the layers of the wet GO membranes. The epoxy spectra do not overlap with water spectra, but the intensity at $\sim$1227 cm^{-1} presents significant oscillations around the corresponding intensity on the dry GO membrane, and the hydroxyl intensity at $\sim$3594 cm^{-1} also shows similar oscillational changes while separated from the band at $\sim$3424 cm^{-1}. Also, we have experimentally confirmed that there is no degradation of the wet GO membranes (see PS12 in the SM). In sharp contrast to the real-time changes in the spectra on the wet GO membrane, we see that the spectra on the fully dry GO membrane remain almost unchanged and overlap together over time (see Fig. 3(a)). Thus, these real-time changes induced by the addition of water indicate the occurrence of spontaneous changes in epoxy and hydroxyl contents at the sampling area on the wet GO membrane. Since the oxygen movements in between the GO layers have large barriers and water adsorption increases interlayer spacings and prevents direct oxygen migration in between GO layer (see PS4 in the SM), these real-time changes observed experimentally mainly reflect the oxygen migration along the basal plane of GO, consistent with the above theoretical prediction.

Notably, the adaptive structural response to the adsorption of biomolecules was further observed. Similarly, the wet GO membranes were *in situ* treated by a saturated cytosine solution droplet of 20 μL for 10 min (see Fig. S7 in the SM), and was analyzed *in situ* by SR-FTIR under ambient conditions. As shown in Fig. 3(b), cytosine has characteristic IR peaks at $\sim$3220 cm^{-1} (H–N–H stretching) and $\sim$1500 cm^{-1} (C–N stretching in C–N ring), and these peaks do not overlap with the above characteristic peaks in the GO spectra, despite overlaps at some other frequencies.[44] Compared with the spectra on the dry and wet GO membranes, we can see significant changes in the intensities at $\sim$1227 cm^{-1}, $\sim$1622 cm^{-1}, and $\sim$3594 cm^{-1} on the wet GO membrane with cytosine adsorbed, indicating large changes in the epoxy and hydroxyl contents. Figure 3(f) presents the corresponding sequent 2D chemical distributions. We find that these chemical contents have been redistributed completely on the wet GO membrane with cytosine adsorbed. Over time, their distributions become even more stable than the distributions on the dry GO membrane. DFT calculations show that the oxygen functional groups may contribute around -30.2 kcal/mol to the binding energy of one cytosine adsorption onto GO. This indicates that adsorbed cytosine strongly interacts with oxygen functional groups to stabilize their distributions on GO (see PS13 in the SM). The conversion from dynamic to stable distributions indicates that the spontaneously dynamic movements of epoxy and hydroxyl on the wet GO membrane possess an adaptive structural response to the cytosine adsorption onto the wet GO membrane; that is, these functional oxygen groups on GO spontaneously break/reform their covalent bonds to adaptively interact with cytosine molecules around their adsorption loci.

In summary, we have theoretically and experimentally shown the water-mediated spontaneously dynamic characteristics of GO under ambient conditions and the structural adaptivity for response to biomolecule adsorption. We note that the isolated local oxygen mobility on GO under electron beam irradiation was observed previously with TEM experiments,[36] and that the spatial structural changes of these oxygen groups on GO can be detected with a room-temperature characteristic relaxation time of about one month[35] or driven with a thermal annealing procedure.[34] Here, we attribute the spontaneously dynamic oxygen migration to the fact that water sharply reduces the barriers of the movements of epoxy and hydroxyl groups to the level less than or comparable to the hydrogen bonding energy in water. Generally, GO structures were observed under a dry or even vacuum condition, e.g., in TEM, STM, or NMR experiments, and a variety of theoretical models of GO structures[17–20] were built, mainly based on static GO structures, e.g., the most popular Lerf–Klinowski model[17] and our recent Shi–Tu model.[19] Clearly, our results present the significant new understanding of GO structures that usually occur in inevitable contact with water in vapor or liquid, e.g., bio-surroundings.

Most importantly, the spontaneously dynamic oxygen migration under ambient conditions actuates the structural adaptivity of GO for response to biomolecule adsorption and scarcely disturbs the biomolecular structures and properties. We also note that GO can interact with a wide range of biomolecules to provide either electrical or optical readouts as biosensors[22–24] as well as can be sensitive to a range of stimuli (pH, gas or biomolecules, or thermal, light, magnetic, or ultrasonic stimuli) to extend its applications as smart platforms in clinical diagnosis and treatment.[26,32,45] Considering that these applications occur usually in touch with water, the adaptive interactions indicated here provide new and crucial insights into the understanding of relevant molecular mechanisms on these applications and also open a new avenue to design adaptive dynamic-responsive systems for expanding relevant applications. Moreover, GO-based resistive switching memories have attracted much attention.[46,47] Since oxygen migration is crucial for the resistive switching behaviors of GO,[47,48] the water-mediated dynamic oxygen migration on GO observed here offers new insights for future design and fabrication of GO-based memresistor devices. Therefore, our new fundamental understanding of graphene oxide as a novel spontaneously dynamic covalent material is of essential importance for the further use of

this material in practical and desirable applications.

We thank Professor Rodney S. Ruoff for his inspiring idea and discussion. We thank Garel Ekoya and Xian Wang for preliminary testing calculations.

References

[1] Wojtecki R J, Meador M A and Rowan S J 2011 *Nat. Mater.* **10** 14
[2] Lehn J M 2015 *Angew. Chem. Int. Ed.* **54** 3276
[3] Lutz J F, Lehn J M, Meijer E W and Matyjaszewski K 2016 *Nat. Rev. Mater.* **1** 16024
[4] Zou W, Dong J, Luo Y, Zhao Q and Xie T 2017 *Adv. Mater.* **29** 1606100
[5] Chang B, Zhang M, Qing G and Sun T 2015 *Small* **11** 1097
[6] Ni C, Zha D, Ye H, Hai Y, Zhou Y, Anslyn E V and You L 2018 *Angew. Chem.* **130** 1314
[7] Ramström O and Lehn J M 2002 *Nat. Rev. Drug Disc.* **1** 26
[8] Stuart M A C, Huck W T S, Genzer J et al 2010 *Nat. Mater.* **9** 101
[9] Jin Y, Yu C, Denman R J and Zhang W 2013 *Chem. Soc. Rev.* **42** 6634
[10] Ong W J and Swager T M 2018 *Nat. Chem.* **10** 1023
[11] Belowich M E and Stoddart J F 2012 *Chem. Soc. Rev.* **41** 2003
[12] Black S P, Sanders J K M and Stefankiewicz A R 2014 *Chem. Soc. Rev.* **43** 1861
[13] Tauk L, Schröder A P, Decher G and Giuseppone N 2009 *Nat. Chem.* **1** 649
[14] Cacciapaglia R, Di Stefano S and Mandolini L 2005 *J. Am. Chem. Soc.* **127** 13666
[15] Lu Y X, Tournilhac F, Leibler L and Guan Z 2012 *J. Am. Chem. Soc.* **134** 8424
[16] Wang Q, Yu C, Zhang C, Long H, Azarnoush S, Jin Y and Zhang W 2016 *Chem. Sci.* **7** 3370
[17] Lerf A, He H, Forster M and Klinowski J 1998 *J. Phys. Chem. B* **102** 4477
[18] Cai W W, Piner R D, Stadermann F J et al 2008 *Science* **321** 1815
[19] Yang J, Shi G, Tu Y and Fang H 2014 *Angew. Chem. Int. Ed.* **53** 10190
[20] Berkesi O, Josepovits K, Sanakis Y, Petridis D and Dékány I 2006 *Chem. Mater.* **18** 2740
[21] Fu W Y, Jiang L, van Geest E P, Lima L M C and Schneider G F 2017 *Adv. Mater.* **29** 1603610
[22] Liu Y, Dong X and Chen P 2012 *Chem. Soc. Rev.* **41** 2283
[23] Morales-Narváez E and Merkoçci A 2018 *Adv. Mater.* **31** 1805043
[24] Loh K P, Bao Q, Eda G and Chhowalla M 2010 *Nat. Chem.* **2** 1015
[25] Deng D, Novoselov K S, Fu Q, Zheng N, Tian Z and Bao X 2016 *Nat. Nanotechnol.* **11** 218
[26] Gu Z J, Zhu S, Yan L, Zhao F and Zhao Y L 2019 *Adv. Mater.* **31** 27 1800662
[27] Kostarelos K 2016 *Nat. Rev. Mater.* **1** 16084
[28] Tu Y, Lv M, Xiu P et al 2013 *Nat. Nanotechnol.* **8** 594
[29] Bitounis D, Ali-Boucetta H, Hong B H, Min D H and Kostarelos K 2013 *Adv. Mater.* **25** 2258
[30] Chen L, Shi G S, Shen J et al 2017 *Nature* **550** 380
[31] Vlassiouk I V 2017 *Nat. Nanotechnol.* **12** 1022
[32] Yu X, Cheng H, Zhang M, Zhao Y, Qu L and Shi G 2017 *Nat. Rev. Mater.* **2** 17046
[33] Novoselov K S, Falko V I, Colombo L, Gellert P R, Schwab M G and Kim K 2012 *Nature* **490** 192
[34] Kumar P V, Bardhan N M, Tongay S, Wu J, Belcher A M and Grossman J C 2014 *Nat. Chem.* **6** 151
[35] Kim S, Zhou S, Hu Y et al 2012 *Nat. Mater.* **11** 544
[36] Erickson K, Erni R, Lee Z, Alem N, Gannett W and Zettl A 2010 *Adv. Mater.* **22** 4467
[37] Suresh S J and Naik V M 2000 *J. Chem. Phys.* **113** 9727
[38] Hummers W S and Offeman R E 1958 *J. Am. Chem. Soc.* **80** 1339
[39] Xu Y, Bai H, Lu G, Li C and Shi G 2008 *J. Am. Chem. Soc.* **130** 5856
[40] Pan D, Wang S, Zhao B, Wu M, Zhang H, Wang Y and Jiao Z 2009 *Chem. Mater.* **21** 3136
[41] Dikin D A, Stankovich S, Zimney E J, Piner R D, Dommett G H B, Evmenenko G, Nguyen S T and Ruoff R S 2007 *Nature* **448** 457
[42] Hontoria-Lucas C, López-Peinado A J, López-González D, Rojas-Cervantes M L and Martín-Aranda R M 1995 *Carbon* **33** 1585
[43] Acik M, Lee G, Mattevi C, Pirkle A, Wallace R M, Chhowalla M, Cho K and Chabal Y 2011 *J. Phys. Chem. C* **115** 19761
[44] Mathlouthi M, Seuvre A M and Koenig J L 1986 *Carbohydr. Res.* **146** 1
[45] Kostarelos K and Novoselov K S 2014 *Nat. Nanotechnol.* **9** 744
[46] Porro S, Accornero E, Pirri C F and Ricciardi C 2015 *Carbon* **85** 383
[47] Kim S K, Kim J Y, Jang B C, Cho M S, Choi S Y, Lee J Y and Jeong H Y 2016 *Adv. Funct. Mater.* **26** 7406
[48] Liu J, Yin Z, Cao X, Zhao F, Wang L, Huang W and Zhang H 2013 *Adv. Mater.* **25** 233

Supplemental Material: Water-mediated spontaneously dynamic oxygen migration on graphene oxide with structural adaptivity for biomolecule adsorption

Yusong Tu (涂育松)[1,2,*], Liang Zhao (赵亮)[1], Jiajia Sun (孙佳佳)[1], Yuanyan Wu (吴园燕)[1], Xiaojie Zhou (周晓洁)[3], Liang Chen (陈亮)[4], Xiaoling Lei (雷晓玲)[5,6], Haiping Fang(方海平)[5,6], Guosheng Shi (石国升)[7,*]

[1]*College of Physics Science and Technology, Yangzhou University, Jiangsu 225009, China*
[2]*Key Laboratory of Polar Materials and Devices, Ministry of Education, Department of optoelectronics, East China Normal University, Shanghai 200062, China*
[3]*National Facility for Protein Science in Shanghai, Shanghai Advanced Research Institute, Chinese Academy of Sciences, Shanghai 201210, China*
[4]*Department of Optical Engineering, Zhejiang A&F University, Lin'an 311300, China*
[5]*Department of Physics, East China University of Science and Technology, Shanghai 200237, China*
[6]*Division of Interfacial Water and Key Laboratory of Interfacial Physics and Technology, Shanghai Institute of Applied Physics, Chinese Academy of Sciences, Shanghai 201800, China*
[7]*Shanghai Applied Radiation Institute, Shanghai University, Shanghai 200444, China*

[*]Email: ystu@yzu.edu.cn; gsshi@shu.edu.cn

Contents:

PS1: Density functional theory (DFT) calculations

PS2: Oxygen migration reactions on GO

PS3: Oxygen migration pathways with two water adsorbed on GO and reaction barriers with respect to the number of adsorbed water molecules

PS4: Possible oxygen migration pathways in between GO layers

PS5: Unbiased ab initio molecular dynamics (AIMD) simulations

PS6: Instruction to the Movie S1

PS7: Reaction pathway of oxygen migration on GO with a local conformation analogous to the conformation in our AIMD simulation

PS8: Measurement method of *in situ* synchrotron radiation-based Fourier transform infrared microscope (SR-FTIR)

PS9: Fabrication of dry GO membranes, wet GO membranes, and wet GO membranes with cytosine adsorbed, supported by BaF_2 substrate

PS10: *In situ* SR-FTIR spectra and sequences of *in situ* images for 2D chemical distributions on GO membranes for two hours

PS11: *In situ* SR-FTIR spectrum and sequence of *in situ* images for 2D chemical distributions on a fully dry GO membrane hermetically sealed in a homemade container where dry nitrogen environment was maintained

PS12: No degradation of GO membranes induced by the addition of water to GO membranes

PS13: Binding energy of cytosine onto GO

PS1: Density functional theory (DFT) calculations

The DFT calculations were performed with the Gaussian 09 software package[S1] to analyse the reaction pathways of oxygen migration in epoxy and hydroxyl groups on the basal plane of GO. All geometry optimizations and frequency calculations were performed at the B3LYP/6-31G(d) level of theory[S2]. Intrinsic reaction coordinate (IRC) calculations were performed on every transition state to confirm that the transition states connect the minima of interest[S3]. As the convergence criteria, a maximum step size is 0.0018 a.u. and a root mean square (RMS) force is 0.0003 a.u.

PS2: Oxygen migration reactions on GO

To analyse the oxygen migration on GO, we consider the movements of epoxy and hydroxyl groups on GO, mainly because they dominate in the oxygen-containing functional groups on the basal plane [S4-S7]. In the most popular Lerf-Klinowski model, the GO structure has a molecular formula of $C_{10}O_1(OH)_1(COOH)_{0.5}$ with 1 epoxy group and 1 hydroxyl group on both sides of graphene basal plane and 0.5 carboxyl groups on the graphene edges, also regarded as reflecting a typical and likely outcome of a standard oxidation process by Hummers methods [S8-S10]. Therefore, it is appropriate to simplify the oxygen-containing functional groups on GO as just epoxy and hydroxyl groups to analyze the oxygen migration on GO.

Meanwhile, we note that on GO the epoxy has two covalent bonds with two carbon atoms and the hydroxyl has one covalent bond with one carbon atom, and their movements are usually involved with the C-O bond breaking/reforming reactions or the proton transfer between the neighboring epoxy and hydroxyl for the exchange between them [S11,S12]. Therefore, we adopt the C-O bond reaction pathway for epoxy movement, and the proton transfer pathway between the epoxy and hydroxyl for the exchange and analyse the oxygen migration on the basal plane of GO.

PS3: Oxygen migration pathways with two water molecules adsorbed on GO and reaction barriers with respect to the number of adsorbed water molecules

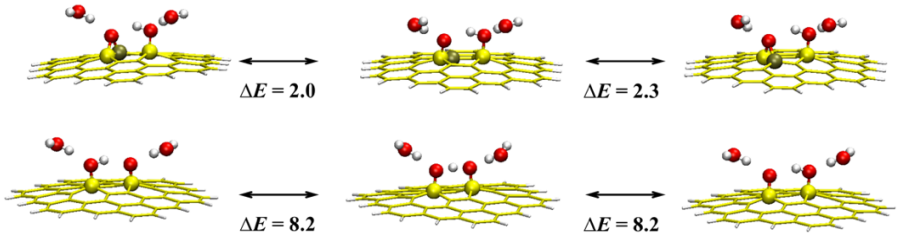

FIG. S1. Oxygen migration pathways with two water adsorbed on GO. The epoxy assisted with the hydroxyl moves by C-O bond breaking/reforming (Path I, black) and the hydroxyl moves by proton transfer to the epoxy and exchange with each other. The numbers indicate the relevant energy barriers with units kcal mol^{-1}. Atom representations and color settings are as in Fig. 1 in the context.

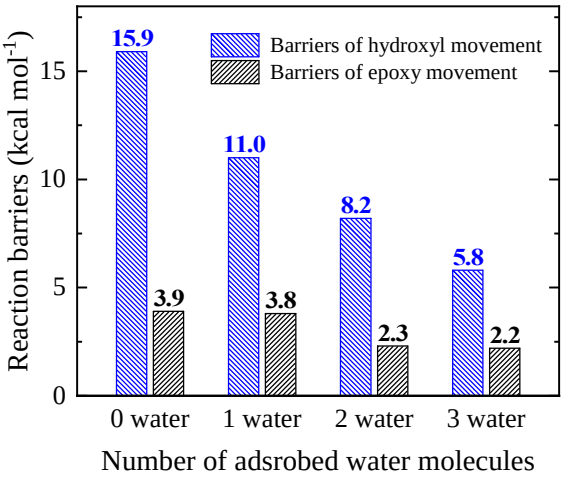

FIG. S2. Reaction barriers of the movements of epoxy (black) and hydroxyl (blue) groups with respect to the number of adsorbed water molecules. The numbers indicate the barrier values with a unit of kcal/mol.

PS4: Possible oxygen migration pathways in between GO layers

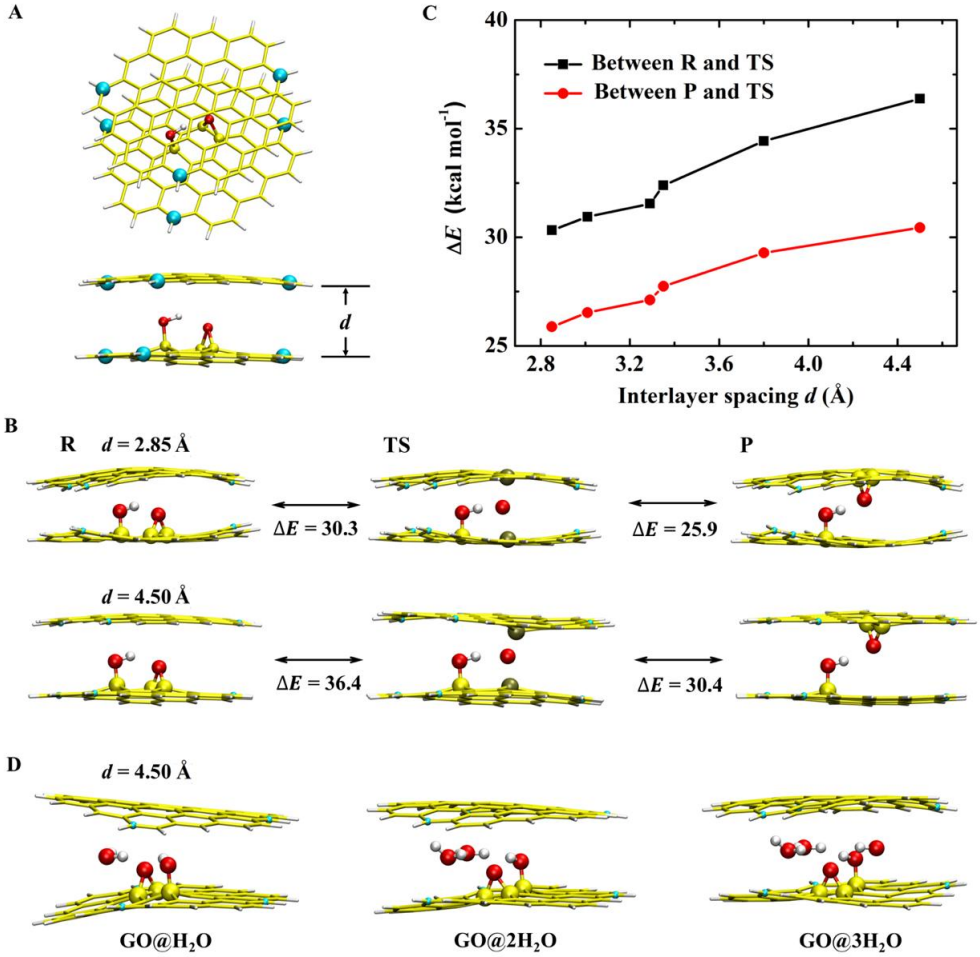

FIG. S3. (A) System of two layers GO. Three carbon atoms on the edge of each layer GO are constrained with pre-set interlayer distances (*d*) to mimic different interlayer spacings in stacked structures of multi-layer GO membranes. The GOs are shown with light yellow lines, and three constrained carbon atoms, as big cyan spheres; the epoxy, hydroxyl, and carbon bonded with them are shown as small coloured spheres (C: yellow, O: red, and H: white). (B) Reaction pathways of epoxy movement in between GO layers with interlayer spacings (*d*) of 2.85 Å and 4.5 Å. Notation: relevant reactants (R), transition states (TS), and products (P), and the numbers indicate the relevant energy barriers with units kcal mol^{-1}. Atom representations and colour settings are the same as in (A), but the constrained carbon atoms are shown with small cyan spheres; the epoxy, hydroxyl, and carbon bonded with them, with big coloured spheres; carbon atoms in reaction transition states, with big tan spheres. (C) Dependence of energy barriers in reaction pathways of epoxy movements in between GO layers on their interlayer spacings (*d*). (D) Optimized geometries of two layers GO with one, two, three adsorbed water molecules for the preset spacing of 4.5 Å.

DFT calculations were performed to analyse the C-O bond reactions in the configuration of neighbouring epoxy and hydroxyl groups for possible oxygen movements in between GO layers. Figure S3A shows the system of two layers GO in DFT calculations. Herein, three carbon atoms on the edge of each layer GO are constrained with pre-set interlayer distances (*d*) to mimic different interlayer spacings in stacked structures of multi-layer GO membranes. As shown in Fig. S3B and S3C, the C-O bond reactions for epoxy movement in between the GO layers have large barriers (at least 25.9 kcal mol^{-1}), and the barrier increases gradually as the interlayer spacing becomes larger. In fact, we failed to achieve the reaction pathway with the interlayer spacing larger than 4.5 Å. Further, we considered water molecules to be adsorbed between the layers of GO. Fig. S3D presents the optimized geometries with one, two, three adsorbed water molecules. We see that water molecules push away these two GO layers and cause their larger spacings. Previous experiments showed the interlayer spacings of GO membranes were usually observed to be around 8-9 Å [S13,S14]. On the other hand, Fig. S4 presents the proton transfer reactions between the epoxy and hydroxyl in between the GO layers. Without water adsorbed, the proton transfer has an energy barrier of 21.6 kcal mol^{-1}; with three water molecules adsorbed, this barrier is sharply reduced down to 12 kcal mol^{-1}. In short, these analyses above indicate that the water adsorption is favourable to the proton transfer for the exchange of the epoxy and hydroxyl in between GO layers, but increases the interlayer spacings and prevents the direct oxygen migration in between GO layers.

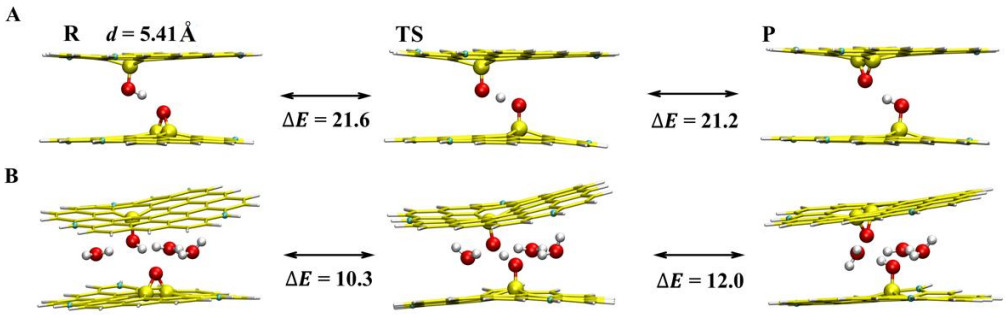

FIG. S4. Pathways of proton transfer reactions between the epoxy and hydroxyl in between the GO layers with pre-set interlayer distances of *d* = 5.41 Å, without or with water adsorbed. The numbers indicate the relevant energy barriers with units kcal mol^{-1}. Atom representations and color settings are as in Fig. S1.

PS5: Unbiased ab initio molecular dynamics (AIMD) simulations

The AIMD simulations were performed with the CP2K 4.1 packages[S15]. We adopted a hybrid Gaussian and plane waves scheme[S16] in DFT implemented in the subroutine QUICKSTEP[S16], and the electronic density is expanded in the form of plane waves with a cut-off of 460 Ry. Double-zeta split valance basis sets are used for all atomic kinds. We used the revised Perdew-Burke-Ernzerh (revPBE)[S17] for the exchange and correlation functional. Grimme D3 dispersion correction are used[S18]. In the AIMD simulations, the self-consistent field convergence criterion was chosen as 10^{-6} a.u. The NVT ensemble was used with a time step of 0.5 fs, and the temperature was maintained at 300 K by a Nosé–Hoover thermostat with a time constant of 0.1 ps.

The simulation system contained one periodic structure of GO in a cubic box with the xyz dimensions of $14.76 \times 17.04 \times 21.02$ $Å^3$ filled with 144 water molecules, and periodic boundary conditions were imposed on all three directions. Such settings lead to a density of of ~1.0 g/mL at positions far from GO surface to mimic liquid water at ambient conditions. The GO nanosheet was constructed with 96 carbon atoms and 7 epoxy groups and 7 hydroxyl groups, based on the Shi-Tu structure model[S19], and it was assigned along the xy directions. Multiple steps were applied to optimize the whole system. We first performed classic MD simulations to equilibrate the systems with the frozen structure of GO for periods of 10 ns using the SPCE water model and the GO force field consistent with our previous studies[S20]. We further fixed the GO structure and then released it to successively twice perform the global geometry optimization of the systems with the CP2K 4.1 packages. The eventual optimized systems were applied as the initial structures to run the AIMD simulations.

PS6: Instruction to the Movie S1

The **Movie S1**, dynamic_GO_water.mov, shows the processes of oxygen migration in epoxy and hydroxyl groups on the basal plane of GO, in our unbiased ab initio molecular dynamics (AIMD) simulation. Water molecule is shown, which has its hydrogen atom located at a distance from the oxygen atoms in oxygen groups at a reaction location less than 3.0 Å. Their hydrogen atoms are linked to the oxygen atoms by blue dashed lines. Atom representations and color settings are as in Fig. 2 in the context, besides other water molecules in environments shown in lines.

PS7: Reaction pathway of oxygen migration on GO with a local conformation analogous to the conformation in our AIMD simulations

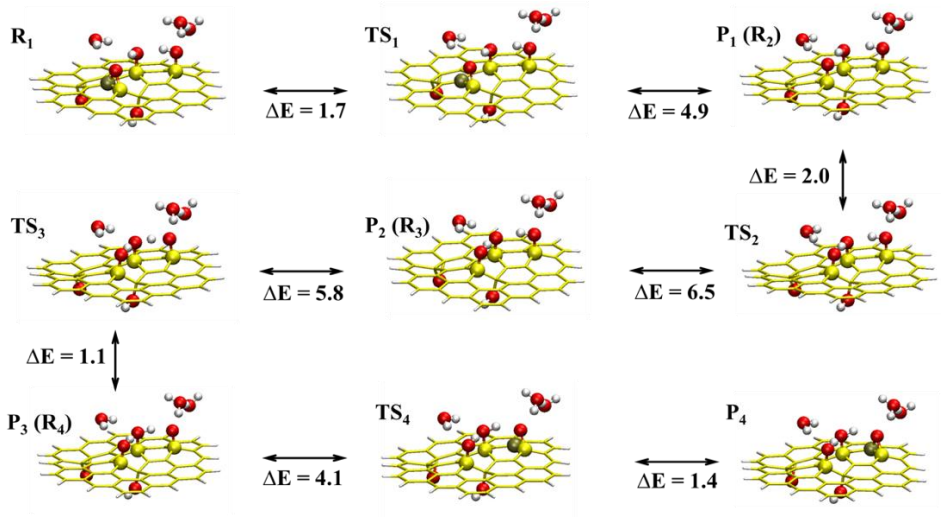

FIG. S5. Reaction pathway of oxygen migration on the basal plane of GO. The local conformation of GO is analogous to the conformation in our AIMD simulation. The oxygen migration process includes two C-O bond breaking/reforming reactions and two proton-transfer reactions. The numbers indicate the relevant energy barriers with units kcal mol^{-1}. Atom representations and color settings are as in Fig. 1 in the context.

PS8: Measurement method of *in situ* synchrotron radiation-based Fourier transform infrared microscope (SR-FTIR)

All the SR-FTIR measurements were performed via infrared micro-spectroscopy and imaging instruments (BL01B beamline of National Facility for Protein Science in Shanghai [NFPS] at Shanghai Synchrotron Radiation Facility [SSRF]). The data collection and instrument operation were controlled by Thermo Scientific OMNIC Atlμs software. The transmission SR-FTIR spectra were collected in the mid-infrared range of 4000–800 cm^{-1}, using the ThermoFisher Nicolet Continuμm XL microscope equipped with a liquid nitrogen–cooled MCT/A detector and a 32×/NA0.65 Reflachromat objective lens via the area map mode. The mapping area was 30×30 μm^2 and was defined by a grid of 4 × 4 discrete spots. Each spot was scanned 16 times with a spectral resolution of 4 cm^{-1}. The aperture size was 20 μm and the scanning step was 10 μm. A mapping was finished when 16 spots within the mapping area were all automatically scanned, exhausting about 3 minutes. The background was collected through a blank BaF_2 substrate before the *in situ* measurement.

Dry graphene oxide (GO) membranes, wet GO membranes, and wet GO membranes with cytosine were measured with *in situ* SR-FTIR. Figure S6 presents a schematic of an original oxygen distribution on a GO, the static oxygen distribution on the dry GO, the dynamic oxygen migration on the wet GO and the adaptive oxygen distribution on the wet GO with adsorbed biomolecules.

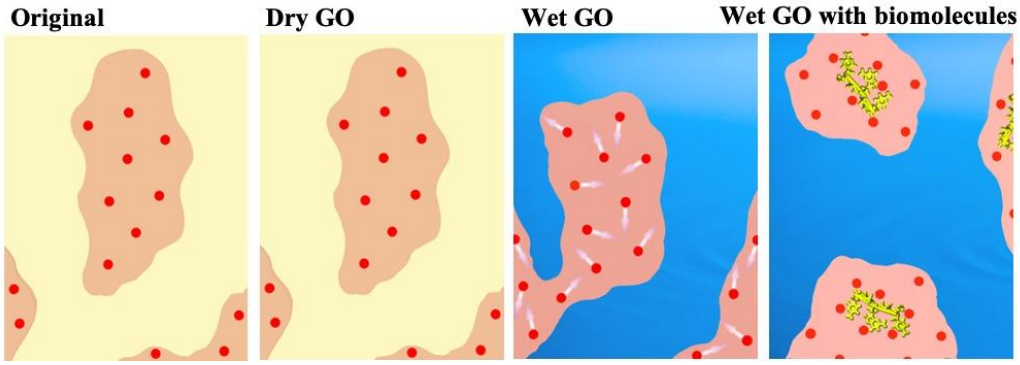

FIG. S6. A schematic of an original oxygen distribution on a GO, the static oxygen distribution on the dry GO, the dynamic oxygen migration on the wet GO and the adaptive oxygen distribution on the wet GO with adsorbed biomolecules. Light red areas with red cycles indicate the oxidised regions of GO with functional oxygen groups and yellow lines represent biomolecules adsorbed on GO. The arrows represent the mobility of oxygen groups on GO.

PS9: Fabrication of dry GO membranes, wet GO membranes, and wet GO membranes with cytosine adsorbed, supported by BaF_2 substrate

Fabrication of dry GO membranes. Graphene oxide (GO) suspension were prepared from natural graphite powder via a modified Hummers method[S13,S21-S23]. We put graphite powders into concentrated H_2SO_4, $K_2S_2O_8$, and P_2O_5 solution with continuous stirring for several hours. Next, we diluted the mixture with deionized water (DI), centrifuged, and washed with DI water, and obtained the preoxidized graphite after drying process. Further oxidization treatments were performed in concentrated H_2SO_4 and $KMnO_4$, diluted with DI water, followed by the addition of 30% H_2O_2. In order to remove ion species, the product was centrifuged and washed sequentially with 1:10 HCl aqueous solution and DI water. Eventually, by centrifugation at 4000 rpm, few-layer graphene oxide was separated to obtain graphene oxide (GO) suspension.

10 μl GO suspension with concentration of 5 mg/ml was deposited on the surface of BaF_2 substrate via a drop-casting method to produce a GO membrane. The GO membrane was dried under an infrared lamp for about 30 minutes.

Fabrication of wet GO membranes. The dry GO membranes were placed on the stage of the SR-FTIR and were measured. After the measurements, the dry GO membranes were wetted *in situ*, as presented in Fig. S7. At first, the dry GO membranes were immersed in a deionized water

droplet of 20 μl for ~10 min, and then, they were covered by only a thin water film for ~ 15 min after the redundant water of the droplet was removed with an absorbent paper. The wet GO membranes were measured *in situ* with SR-FTIR.

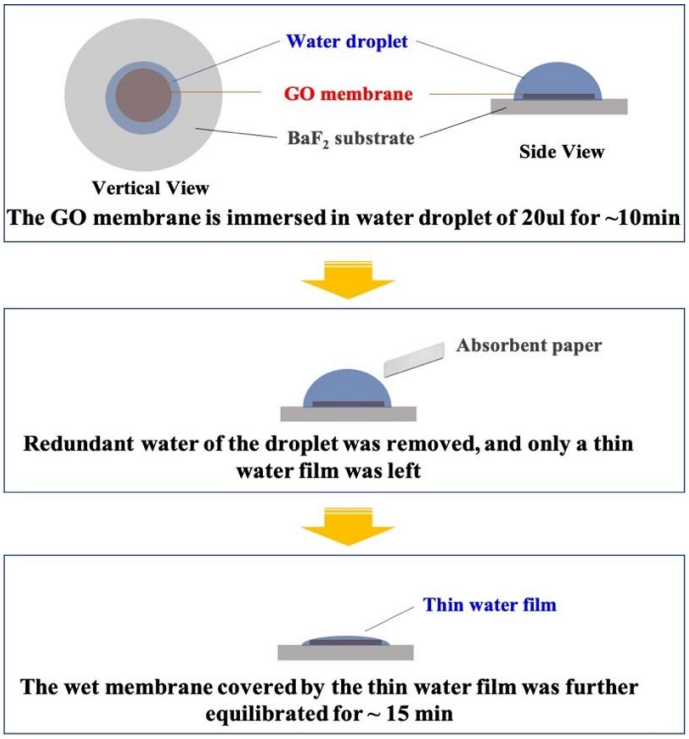

FIG. S7. Fabrication schematic of wet GO membranes.

Fabrication of wet GO membranes with cytosine adsorbed. After the measurements on wet GO membranes, the wet GO membranes were subsequently adsorbed with cytosine *in situ*. With the similar way shown in Fig. S7, the wet GO membranes were immersed in a saturated cytosine solution droplet of 20 μl (7.69g/L at room temperature) for ~10 min. Then, they were covered by only a thin solution film for ~ 15 min after the redundant solution of the droplet was removed with an absorbent paper. The wet GO membranes with cytosine adsorbed were measured *in situ* with SR-FTIR.

PS10: *In situ* SR-FTIR spectra and sequences of *in situ* images for 2D chemical distributions on GO membranes for two hours

In situ SR-FTIR spectroscopy experiments for two hours were performed to check the dynamic oxygen migration over an area of 30 × 30 μm^2 of GO membranes (Fig. S8-S11) and over a larger over a larger area of 90 × 90 μm^2 of GO membranes (Fig. S12-S15).

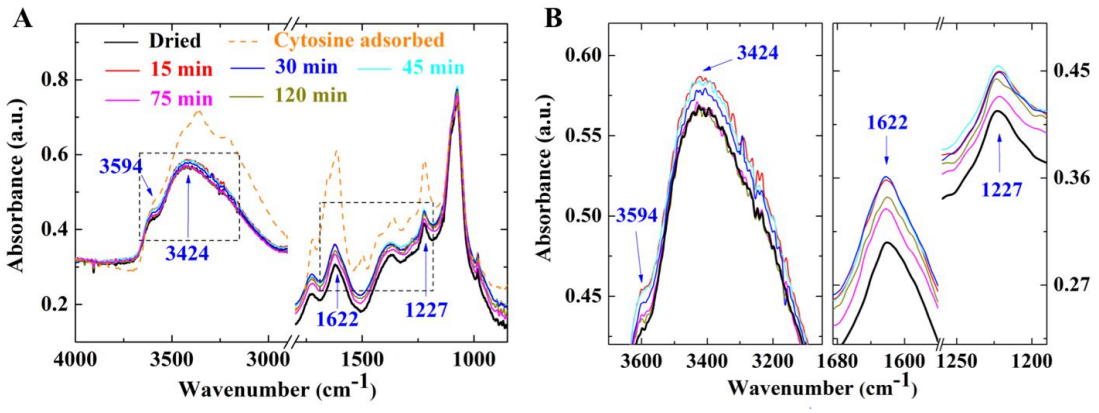

FIG. S8. *In situ* SR-FTIR spectroscopy measurements over an area of 30 × 30 μm^2 of GO membranes for two hours. (A**)** *In situ* SR-FTIR spectrum acquired, from a dry GO membrane (black), from the wet GO membrane (colour based on time), and from the wet GO membrane with cytosine adsorbed (orange, dashed). (B**)** Enlargements of the spectrum for two dotted-box regions of interest from the wet GO membrane shown in A. Characteristic IR peaks occur in the GO spectra at ~1227 cm^{-1} (C-O-C stretching vibration of epoxy), ~1622 cm^{-1} (C=C stretching of aromatic ring and deformation vibration of adsorbed water), ~3424 cm^{-1} (O-H stretching vibration of adsorbed water), and ~3594 cm^{-1} (O-H stretching of hydroxyl), and peaks occur in the spectra of GO with cytosine adsorbed at ~3220 cm^{-1} (H-N-H stretching) and 1500 cm^{-1} (C-N stretching in C-N ring).

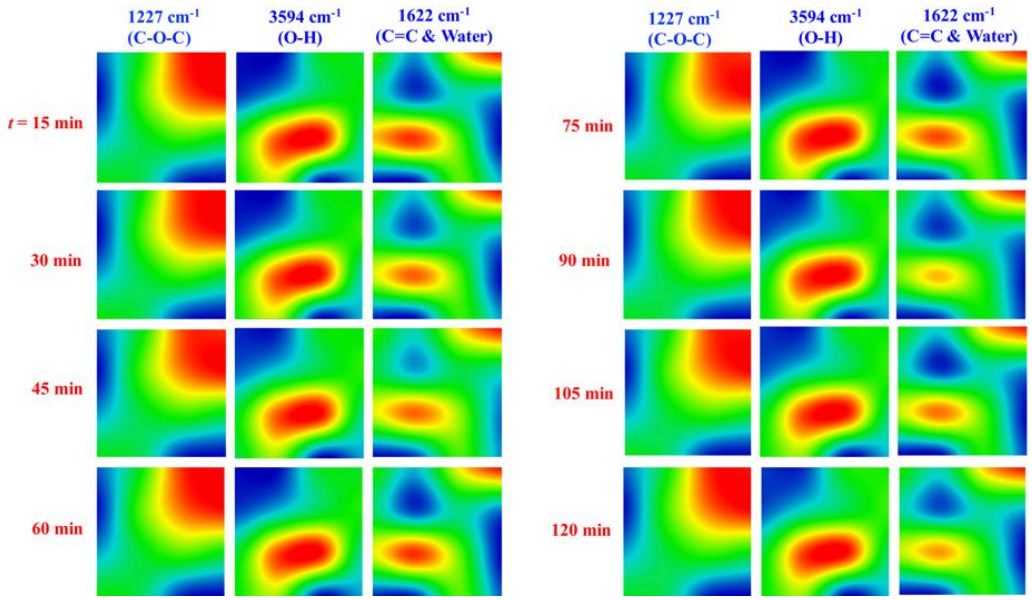

FIG. S9. Sequence of *in situ* images for 2D chemical distributions over the sampling area on the dry GO membrane at 1227 cm^{-1}, 1622 cm^{-1}, and 3594 cm^{-1}. The left numbers denote the time of the sequence with units minute.

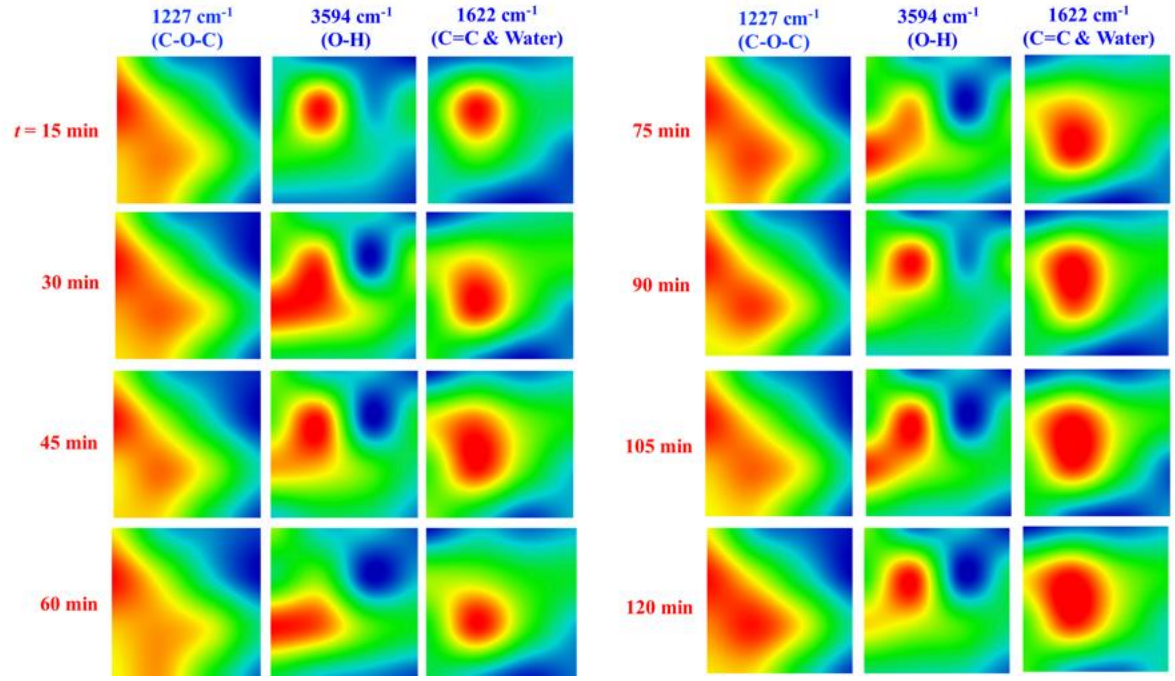

FIG. S10. Sequence of *in situ* images for 2D chemical distributions over the sampling area on a wet GO membrane at 1227 cm^{-1}, 1622 cm^{-1}, and 3594 cm^{-1} for two hours.

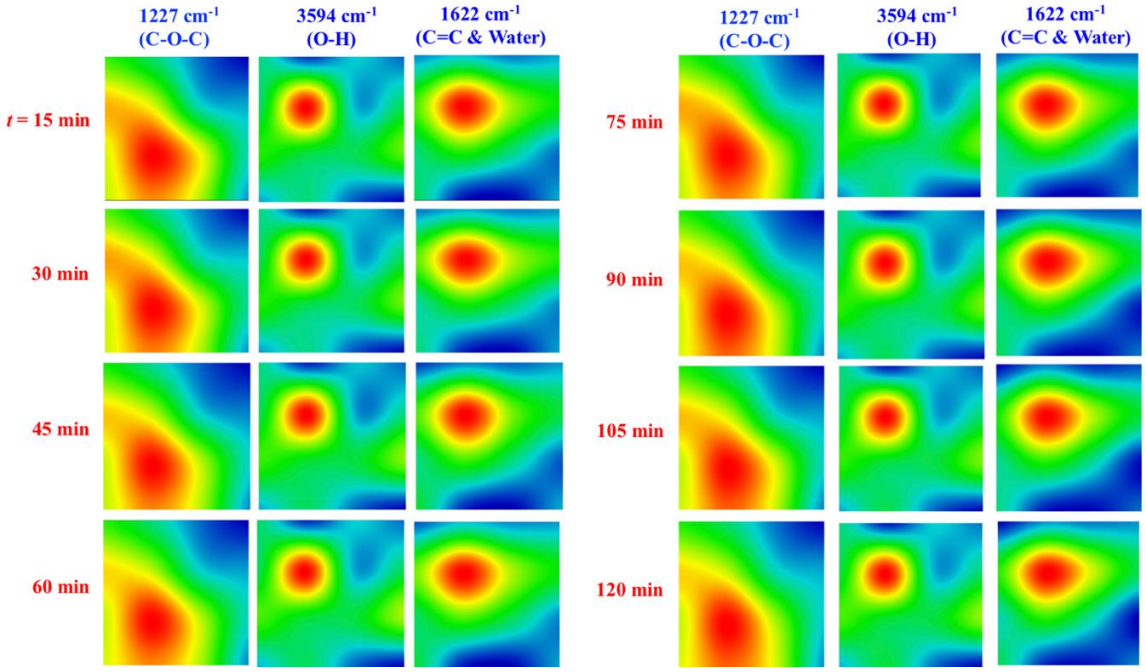

FIG. S11. Sequence of *in situ* images for 2D chemical distributions over the sampling area of the wet GO membrane with cytosine adsorbed at frequencies of 1227 cm^{-1}, 1622 cm^{-1} and 3594 cm^{-1}.

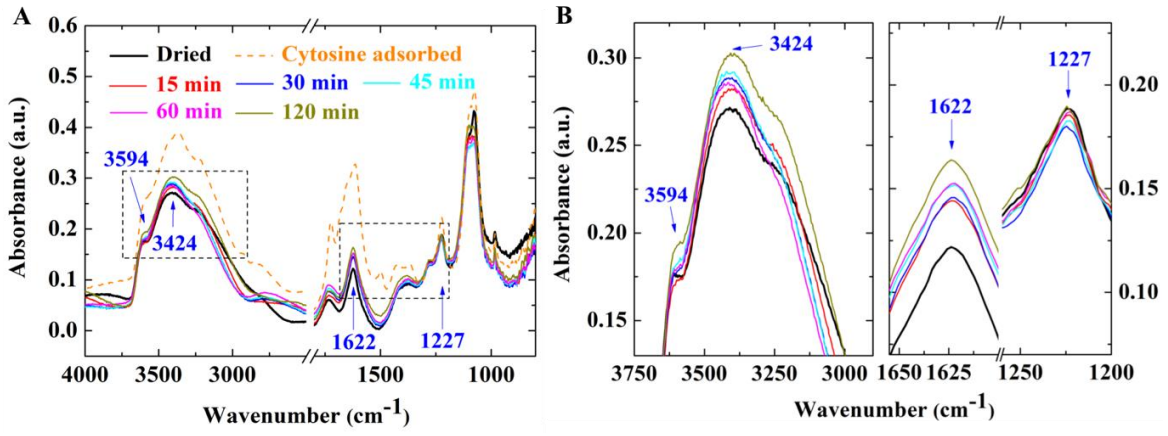

FIG. S12. *In situ* SR-FTIR spectroscopy measurements over a larger area of 90 × 90 μm^2 of GO membranes. (A**)** *In situ* SR-FTIR spectrum acquired, from a dry GO membrane (black), from the wet GO membrane (colour based on time), and from the wet GO membrane with cytosine adsorbed (orange, dashed). (B**)** Enlargements of the spectrum for two dotted-box regions of interest from the wet GO membrane shown in A. Characteristic IR peaks occur in the GO spectra at ~1227 cm^{-1} (C-O-C stretching vibration of epoxy), ~1622 cm^{-1} (C=C stretching of aromatic ring and deformation vibration of adsorbed water), ~3424 cm^{-1} (O-H stretching vibration of adsorbed water), and ~3594 cm^{-1} (O-H stretching of hydroxyl), and peaks occur in the spectra of GO with cytosine adsorbed at ~3220 cm^{-1} (H-N-H stretching) and 1500 cm^{-1} (C-N stretching in C-N ring).

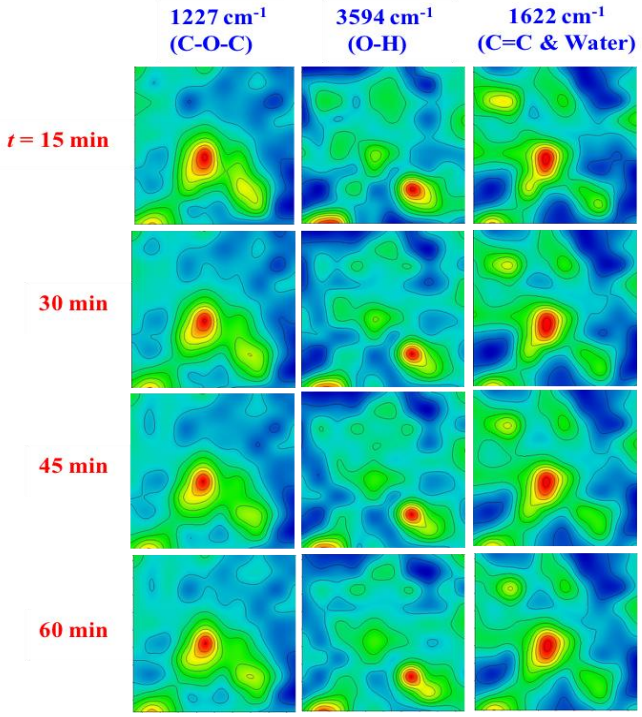

FIG. S13. Sequence of *in situ* images for 2D chemical distributions over a larger area of 90 × 90 μm^2 of the dry GO membrane, at frequencies of 1227 cm^{-1}, 1622 cm^{-1} and 3594 cm^{-1}.

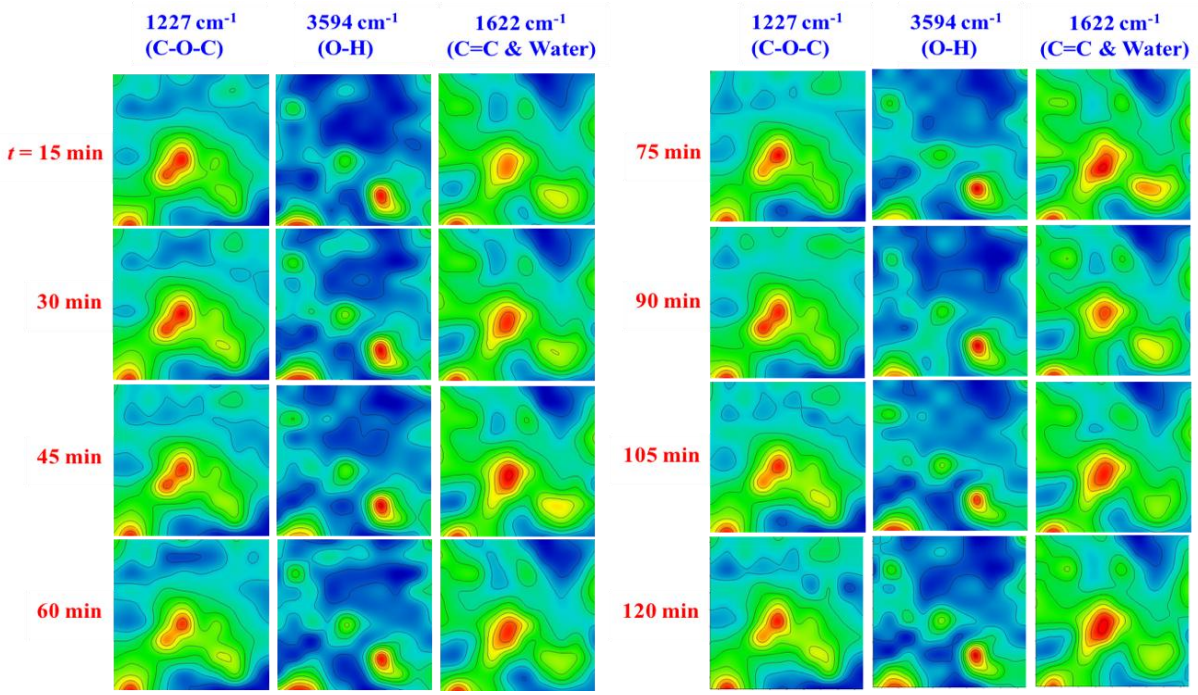

FIG. S14. Sequence of *in situ* images for 2D chemical distributions over a larger area of 90 × 90 μm^2 of the wet GO membrane, at frequencies of 1227 cm^{-1}, 1622 cm^{-1} and 3594 cm^{-1}.

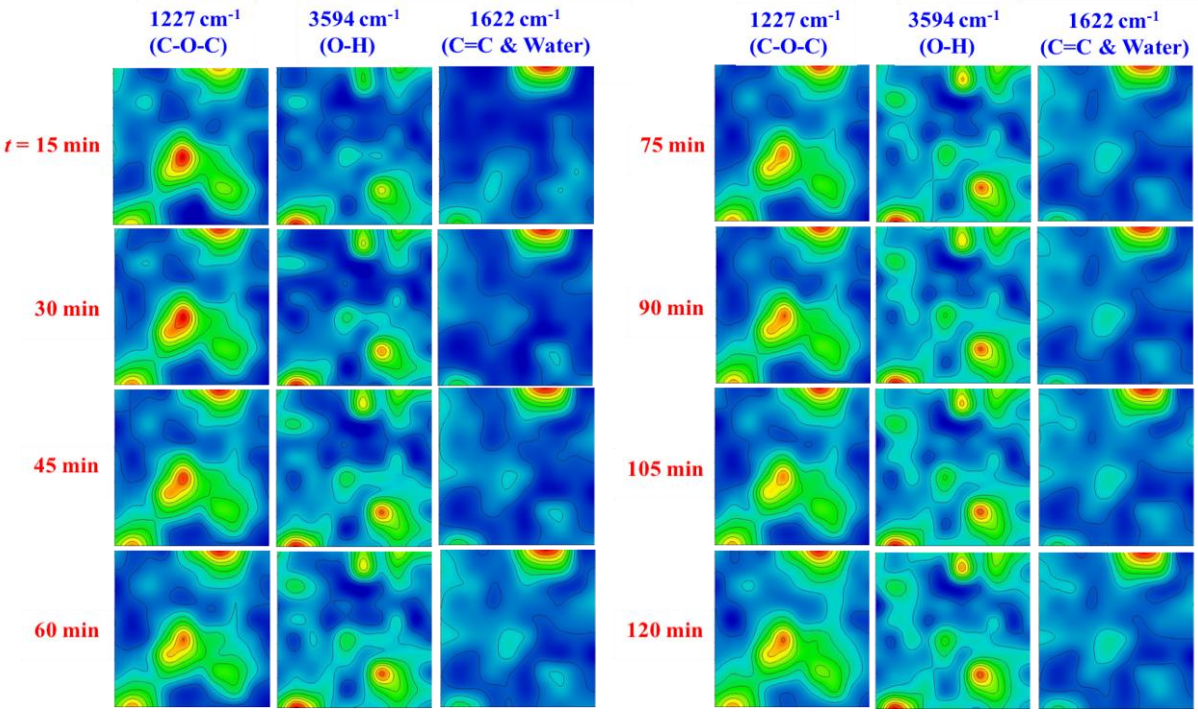

FIG. S15. Sequence of *in situ* images for 2D chemical distributions over a larger area of 90 × 90 μm^2 of the wet GO membrane with cytosine adsorbed, at frequencies of 1227 cm^{-1}, 1622 cm^{-1} and 3594 cm^{-1}.

PS11: *In situ* SR-FTIR spectrum and sequence of *in situ* images for 2D chemical distributions on a fully dry GO membrane hermetically sealed in a homemade container where dry nitrogen environment was maintained

A container with a sample cell was designed and fabricated, in which dry nitrogen environment can be maintained for SR-FTIR measurements (see Fig. S16). The GO membranes were re-prepared inside this container via a drop-casting method. In detail, 10 uL GO suspension was dropped directly on the BaF_2 substrate of this container, and subsequently dried under an infrared lamp for ~ 30 min; the container with the sample was unclosed and put in a glove box filled with nitrogen gas at room temperature for 24 hours; then, the container with the sample was screwed hermetically and filled with nitrogen gas; a weak flow of nitrogen gas went through the container during the SR-FTIR measurements. This whole conducted process ensures GO to avoid being highly hydrated in ambient conditions and be kept at zero RH for spectroscopy measurements.

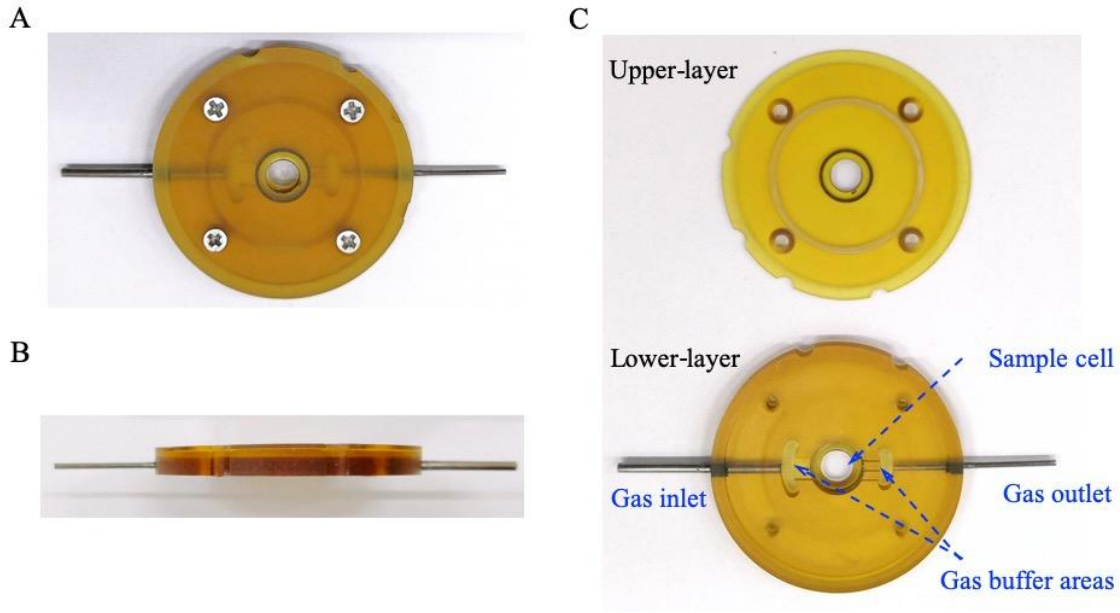

FIG. S16. (A) and (B) The top (A) and side (B) views of a container that is used to seal the sample for its SR-FTIR measurements. (C) The top views of two layers of the unclosed container. These two layers can be screwed and packed together hermetically to provide a sealed sample cell. Two BaF_2 substrates (the transport part of the sample cell) have been constructed with these two layers to afford the window that facilitates SR-FTIR measurements. Nitrogen gas flows from the inlet tube through this cell to the outlet tube and enables the sample to avoid being highly hydrated in ambient conditions.

The spectra measured over an area of 30 × 30 μm^2 on the fully dry GO membrane sealed hermetically in this container with dry nitrogen environment are shown in Fig. S17. We see that the spectra as well as the 2D distributions of the epoxy and hydroxyl contents are almost unchanged with time. They are much more stable than the results measured on the dry GO

membrane exposed in ambient conditions (see Fig. 3B and 3D in the context and Fig. S9 in PS10).

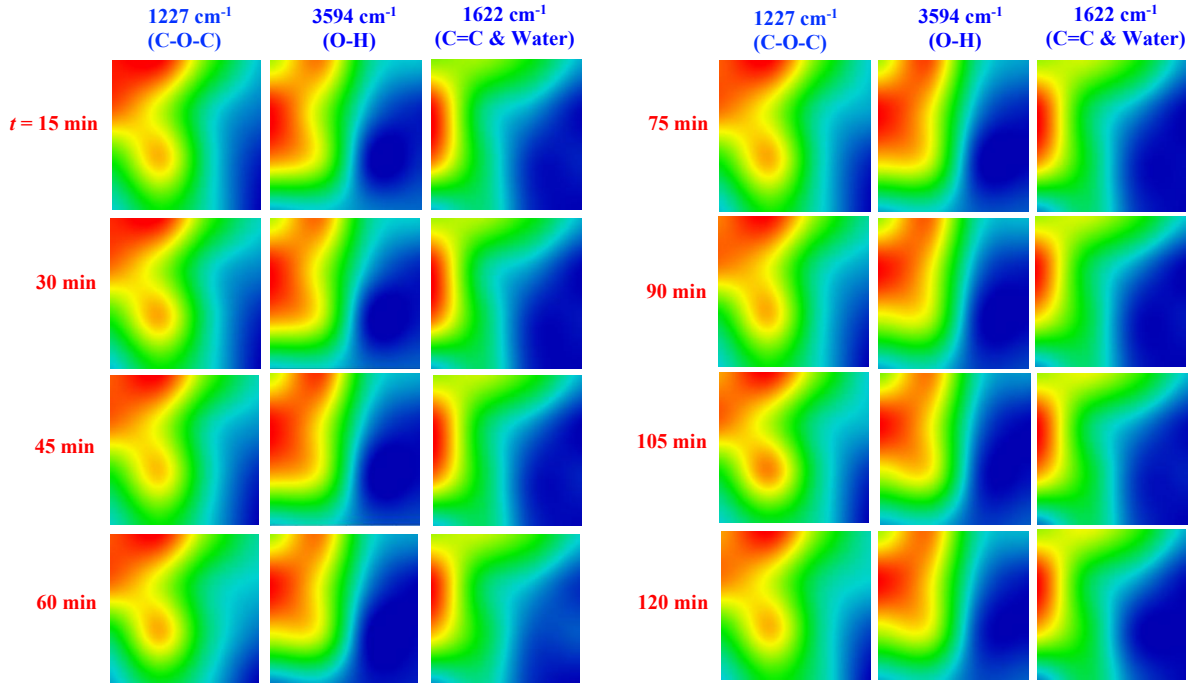

FIG. S17. Sequence of *in situ* images for 2D chemical distributions over the sampling area on the fully dry GO membrane sealed hermetically in the container with dry nitrogen environment at 1227 cm^{-1}, 1622 cm^{-1}, and 3594 cm^{-1}. The left numbers denote the time of the sequence with units minute.

PS12: No degradation of GO membranes induced by the addition of water to GO membranes

Experiments were carried out to check whether or not the addition of water to GO membranes induces the GO degradation. In Fig. S18, we can see that the dry GO membranes present no change of their masses after they were immersed in deionized water for half an hour and then re-dried in a vacuum desiccator at 50 ℃ for 24 hours. This indicates that there is no degradation of the wet GO membranes immersed in water for half an hour.

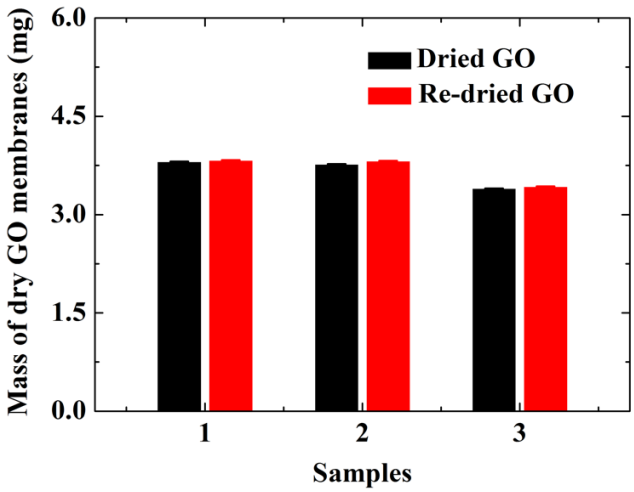

FIG. S18. Comparisons between the masses of dry GO membranes and their masses after they were immersed in deionized water for half an hour and then re-dried in a vacuum desiccator at 50 ℃ for 24 hours.

PS13: Binding energy of cytosine onto GO

DFT calculations were carried out to analyse the interaction between GO and its adsorbed cytosine. Figure S19 shows the optimized geometries of cytosine adsorbed onto both pure graphene and GO. The binding energy of cytosine onto GO can be divided into two parts, i.e., the adsorption of cytosine by graphene itself and the interaction of cytosine with oxygen functional groups. Thus, we have estimated the contribution of oxygen functional groups on GO, by the total binding energy of cytosine onto GO minus the binding energy of cytosine by pure graphene in the following formula,

$$\delta E = (E_{\text{cytosine@GO}} - E_{\text{cytosine}} - E_{\text{GO}}) - (E_{\text{cytosine@graphene}} - E_{\text{cytosine}} - E_{\text{graphene}}).$$

We find, for one cytosine adsorption, δE = –30.2 kcal mol^{-1}, approximately equivalent to five times hydrogen binding energy in two water molecules. This indicates that the adsorbed cytosine strongly interacts with these oxygen functional groups and contributes significantly to the stabilization of their distribution.

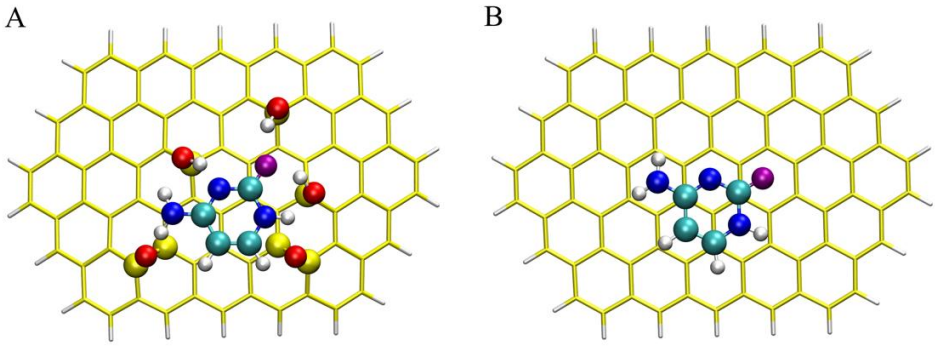

FIG. S19. (A) and (B) Optimized geometries of cytosine adsorbed onto both GO (A) and pure graphene (B). The GO and pure graphene are shown with light yellow lines, and the epoxy, hydroxyl, and carbon bonded with them on GO are shown as coloured spheres (C: yellow, O: red, and H: white); the adsorbed cytosine are also shown as coloured spheres (C: cyan, O: purple, N: blue, and H: white).

SReferences

[S1] M. Frisch *et al.*, Wallingford, CT **19**, 227 (2009).

[S2] A. D. Becke, J. Chem. Phys. **98**, 5648 (1993).

[S3] J. S. F. Jeffrey I. Steinfeld, William L. Hase, *Chemical Kinetics and Dynamics* (Prentice-Hall: Englewood Clitts, NJ, 1989).

[S4] W. Gao, L. B. Alemany, L. Ci, and P. M. Ajayan, Nat. Chem. **1**, 403 (2009).

[S5] W. Cai *et al.*, Science **321**, 1815 (2008).

[S6] C. Gómez-Navarro, J. C. Meyer, R. S. Sundaram, A. Chuvilin, S. Kurasch, M. Burghard, K. Kern, and U. Kaiser, Nano Lett. **10**, 1144 (2010).

[S7] K. Erickson, R. Erni, Z. Lee, N. Alem, W. Gannett, and A. Zettl, Adv. Mater. **22**, 4467 (2010).

[S8] A. Lerf, H. He, M. Forster, and J. Klinowski, J. Phys. Chem. B **102**, 4477 (1998).

[S9] C. J. Shih, S. Lin, R. Sharma, M. S. Strano, and D. Blankschtein, Langmuir **28**, 235 (2012).

[S10] N. V. Medhekar, A. Ramasubramaniam, R. S. Ruoff, and V. B. Shenoy, ACS Nano **4**, 2300 (2010).

[S11] S. Kim, S. Zhou, Y. Hu, M. Acik, Y. J. Chabal, C. Berger, W. de Heer, A. Bongiorno, and E. Riedo, Nat. Mater. **11**, 544 (2012).

[S12] P. V. Kumar, N. M. Bardhan, S. Tongay, J. Wu, A. M. Belcher, and J. C. Grossman, Nat. Chem. **6**, 151 (2014).

[S13] L. Chen *et al.*, Nature **550**, 380 (2017).
[S14] R. K. Joshi, P. Carbone, F. C. Wang, V. G. Kravets, Y. Su, I. V. Grigorieva, H. A. Wu, A. K. Geim, and R. R. Nair, Science **343**, 752 (2014).
[S15] J. Hutter, M. Iannuzzi, F. Schiffmann, and J. VandeVondele, Wiley Interdiscip. Rev. Comput. Mol. Sci. **4**, 15 (2014).
[S16] B. G. LIPPERT, J. H. PARRINELLO, and MICHELE, Mol. Phys. **92**, 477 (1997).
[S17] Y. Zhang and W. Yang, Phys. Rev. Lett. **80**, 890 (1998).
[S18] S. Grimme, J. Antony, S. Ehrlich, and H. Krieg, J. Chem. Phys. **132**, 154104 (2010).
[S19] J. Yang, G. Shi, Y. Tu, and H. Fang, Angew. Chem. Int. Ed. **53**, 10190 (2014).
[S20] Y. Tu *et al.*, Nat. Nanotechnol. **8**, 594 (2013).
[S21] W. S. Hummers and R. E. Offeman, J. Am. Chem. Soc. **80**, 1339 (1958).
[S22] Y. Xu, H. Bai, G. Lu, C. Li, and G. Shi, J. Am. Chem. Soc. **130**, 5856 (2008).
[S23] D. Pan, S. Wang, B. Zhao, M. Wu, H. Zhang, Y. Wang, and Z. Jiao, Chem. Mater. **21**, 3136 (2009).